Received: August 14, 2018 Revised: June 18, 2019 Accepted: June 26, 2019

(onlinelibrary.wiley.com) DOI: 10.1111/ner.13037

Patient-Specific Analysis of Neural Activation During Spinal Cord Stimulation for Pain

Scott F. Lempka, PhD*†‡§¶; Hans J. Zander, BBmE‡¶; Carlos J. Anaya, BS‡¶; Alexandria Wyant, BA*; John G. Ozinga IV PA-C*; Andre G. Machado, MD, PhD*****

Objective: Despite the widespread use of spinal cord stimulation (SCS) for chronic pain management, its neuromodulatory effects remain poorly understood. Computational models provide a valuable tool to study SCS and its effects on axonal pathways within the spinal cord. However, these models must include sufficient detail to correlate model predictions with clinical effects, including patient-specific data. Therefore, the goal of this study was to investigate axonal activation at clinically relevant SCS parameters using a computer model that incorporated patient-specific anatomy and electrode locations.

Methods: We developed a patient-specific computer model for a patient undergoing SCS to treat chronic pain. This computer model consisted of two main components: 1) finite element model of the extracellular voltages generated by SCS and 2) multicompartment cable models of axons in the spinal cord. To determine the potential significance of a patient-specific approach, we also performed simulations with standard canonical models of SCS. We used the computer models to estimate axonal activation at clinically measured sensory, comfort, and discomfort thresholds.

Results: The patient-specific and canonical models predicted significantly different axonal activation. Relative to the canonical models, the patient-specific model predicted sensory threshold estimates that were more consistent with the corresponding clinical measurements. These results suggest that it is important to account for sources of interpatient variability (e.g., anatomy, electrode locations) in model-based analysis of SCS.

Conclusions: This study demonstrates the potential for patient-specific computer models to quantitatively describe the axonal response to SCS and to address scientific questions related to clinical SCS.

Keywords: Chronic pain, computer simulation, failed back surgery syndrome, spinal cord stimulation

Conflict of Interest: Scott F. Lempka holds stock options with Presidio Medical, Inc. and serves on the scientific advisory board. Andre G. Machado has distribution rights to Cardionomic, Inc. and Enspire DBS, Inc. and is a paid consultant of St. Jude Medical. Hans J. Zander, Carlos J. Anaya, Alexandria Wyant, and John G. Ozinga declare no competing interests.

INTRODUCTION

Spinal cord stimulation (SCS) is a common neurostimulation therapy for neuropathic pain conditions (e.g., failed back surgery syndrome, complex regional pain syndrome) that are refractory to conventional treatments (1–3). Although SCS has been a widely used clinical therapy for decades, it still has limited success (~50% of patients receive ≥50% reduction in pain) (3).

To improve clinical outcomes of SCS, we need to better understand the electric fields generated by SCS and their direct effects

Address correspondence to: Scott F. Lempka, PhD, Department of Biomedical Engineering, University of Michigan, 2800 Plymouth Road, NCRC 014-184, Ann Arbor, MI 48104-2800, USA.
lempka@umich.edu

* Center for Neurological Restoration, Cleveland Clinic, Cleveland, OH, USA;
† Research Service, Louis Stokes Cleveland Veterans Affairs Medical Center, Cleveland, OH, USA;
‡ Department of Biomedical Engineering, University of Michigan, Ann Arbor, MI, USA;
§ Department of Anesthesiology, University of Michigan, Ann Arbor, MI, USA;
¶ Biointerfaces Institute, University of Michigan, Ann Arbor, MI, USA; and
** Department of Neurosurgery, Neurological Institute, Cleveland Clinic, Cleveland, OH, USA

For more information on author guidelines, an explanation of our peer review process, and conflict of interest informed consent policies, please go to www.wiley.com/WileyCDA/Section/id-301854.html

Source(s) of financial support: This work was supported by the National Institutes of Health (NIH R01 NS089530) (Hans J. Zander and Scott F. Lempka), the Louis Stokes Cleveland Veterans Affairs Medical Center, Cleveland, OH, USA (Scott F. Lempka), the University of Michigan Rackham Merit Fellowship Program (Carlos J. Anaya), and the Cleveland Clinic Research Program Committees, Cleveland, OH, USA (Scott F. Lempka). This research was supported in part through computational resources and services provided by Advanced Research Computing at the University of Michigan, Ann Arbor, MI, USA.

on the nervous system (4). While experimental and/or clinical studies are useful in studying the mechanisms of action of neurostimulation therapies (4–8), these studies include shortcomings related to interspecifies differences and difficulties in assessing stimulation quality and perception in animal models. In the past, several groups have used computational models to study the bioelectric effects of SCS. These studies have helped improve lead design, stimulation configurations, waveform parameters, and programming procedures (9–13). Computational models have also provided insight into the direct neural response to SCS and its potential mechanisms of action (14–17).

Although these computational studies have been productive, they utilized canonical models with geometric parameters based on average anatomical measurements with the goal of investigating technical and scientific principles that could be generalized to the target patient population. Typically, these generalized models do not account for the interpatient variability in anatomy and electrode locations that has been previously reported (18,19). Clinical experience indicates significant variability in the therapeutic stimulation parameters (e.g., amplitude, pulse width, and stimulation configuration), lead placement, and the degree of efficacy across patients that may limit the utility or accuracy of canonical SCS models in predicting the neural response within individual patients (19–24). To successfully correlate model-based predictions with patient-specific clinical effects, it may be necessary for computer models of SCS to incorporate three-dimensional (3D) patient-specific anatomy and electrode locations. 3D patient-specific computational models have shown tremendous success in defining optimal stimulation parameters and describing potential mechanisms of action in other neurostimulation therapies, such as deep brain stimulation (25–28), but they have not been applied to SCS.

Therefore, the goal of this study was to develop a 3D patient-specific computer model of SCS. We defined the patient-specific model from preoperative and postoperative imaging and electrode impedance measurements for a patient undergoing SCS to treat neuropathic pain. We performed clinical measurements to assess the subject's sensory, comfort, and discomfort thresholds (DTs) across several sets of stimulation parameters (e.g., pulse width and stimulation configuration). We also compared the results derived from the patient-specific computer model to results predicted by canonical models of SCS.

METHODS

Patient Demographics

This study was reviewed and approved by the institutional review board at the Cleveland Clinic (Cleveland, OH, USA). We recruited one patient who was being treated with SCS as part of his standard clinical care and who provided informed consent to participate in the study. The patient was a 37-year-old male, who had been diagnosed with postlaminectomy syndrome with chronic pain in his left leg. Approximately 2 weeks prior to enrollment, a three-column paddle lead array (Medtronic Model 39,565 Specify™ 5–6-5 Surgical Lead, Medtronic, Inc., Minneapolis, MN, USA) had been implanted at the T8-T9 spinal levels and connected to a rechargeable voltage-regulated implantable pulse generator (IPG) (RestoreSensor™ Model 37,714, Medtronic, Inc.).

Clinical Testing

We performed all clinical testing procedures at a single visit approximately 6 weeks after SCS implantation to allow time for encapsulation of the implanted electrode array (29). To localize the electrode array relative to the spine, we obtained a postoperative computed tomography (CT) scan of the lower thoracic spinal levels (see "Model Analysis"). We measured the sensory threshold (ST), comfort threshold (CT), and DT for several sets of stimulation parameters. To determine these thresholds, we followed 5 steps: 1) we increased the amplitude until the participant experienced stimulation-induced paresthesias; 2) we reduced the amplitude until the participant no longer reported paresthesias; 3) we increased the amplitude in 0.1 V increments until the participant experienced paresthesias (defined as the ST); 4) we increased the amplitude until the stimulation became uncomfortable (defined as the DT); and 5) we decreased the amplitude until the stimulation-induced paresthesias were at a maximum intensity that was comfortable to the participant (defined as the CT).

To consider the effects of stimulation parameters on axonal recruitment, we varied the pulse width and the stimulation configuration (10,12). For each set of stimulation parameters, we used a standard pulse frequency of 50 Hz (30). We tested the following pulse widths: 60, 210, 300, 450, and 1000 μs. We tested the following stimulation configurations: bipole, longitudinal guarded cathode, transverse guarded cathode, and pseudo-monopole. We used a single cathode, which had provided the participant with significant pain relief (see the Supplemental Methods, Supporting Information for further details). To help ensure that the spinal cord was in a similar position relative to the spine during both imaging procedures and clinical testing, we performed the testing procedures while the participant was supine on an exam bed.

Because the participant's commercial SCS system utilized voltage-controlled stimulation, we also considered the effects of electrode impedance on stimulation thresholds. At the end of the research testing, we measured the bipolar electrode impedances across the entire array. The average electrode impedance was $695 \pm 34.7\ \Omega$.

Model Analysis

Step 1: Calculate the Extracellular Voltages Generated by SCS

The first step in our model analysis was to estimate the extracellular voltages generated in the spinal cord during SCS. We developed a finite element model (FEM) of the lower thoracic spinal cord and surrounding anatomy based on the patient-specific anatomy and electrode locations. We used preoperative magnetic resonance imaging (MRI) to segment the participant's spinal cord, cerebrospinal fluid (CSF), epidural fat, and spine (Fig. 1). We used the postoperative CT scan to localize the SCS electrodes and segment the participant's spine. We then coregistered the segmented 3D surfaces from the preoperative and postoperative images and defined a patient-specific FEM. This patient-specific FEM included a spinal cord domain scaled to match the anteroposterior and mediolateral dimensions of the participant's spinal cord anatomy at the T9 spinal level and included an explicit representation of the electrode array. The FEM also included a domain to represent the electrode encapsulation that occurs with chronic SCS implants (29). To assess whether or not there is an advantage to the patient-specific approach compared to previously-used canonical models, we also performed simulations with two versions of a canonical FEM. In the first canonical FEM, the same SCS array was placed on the dural surface along the spinal cord midline to resemble previous canonical models of SCS (16,20,31–33). The second canonical FEM was an "impedance-

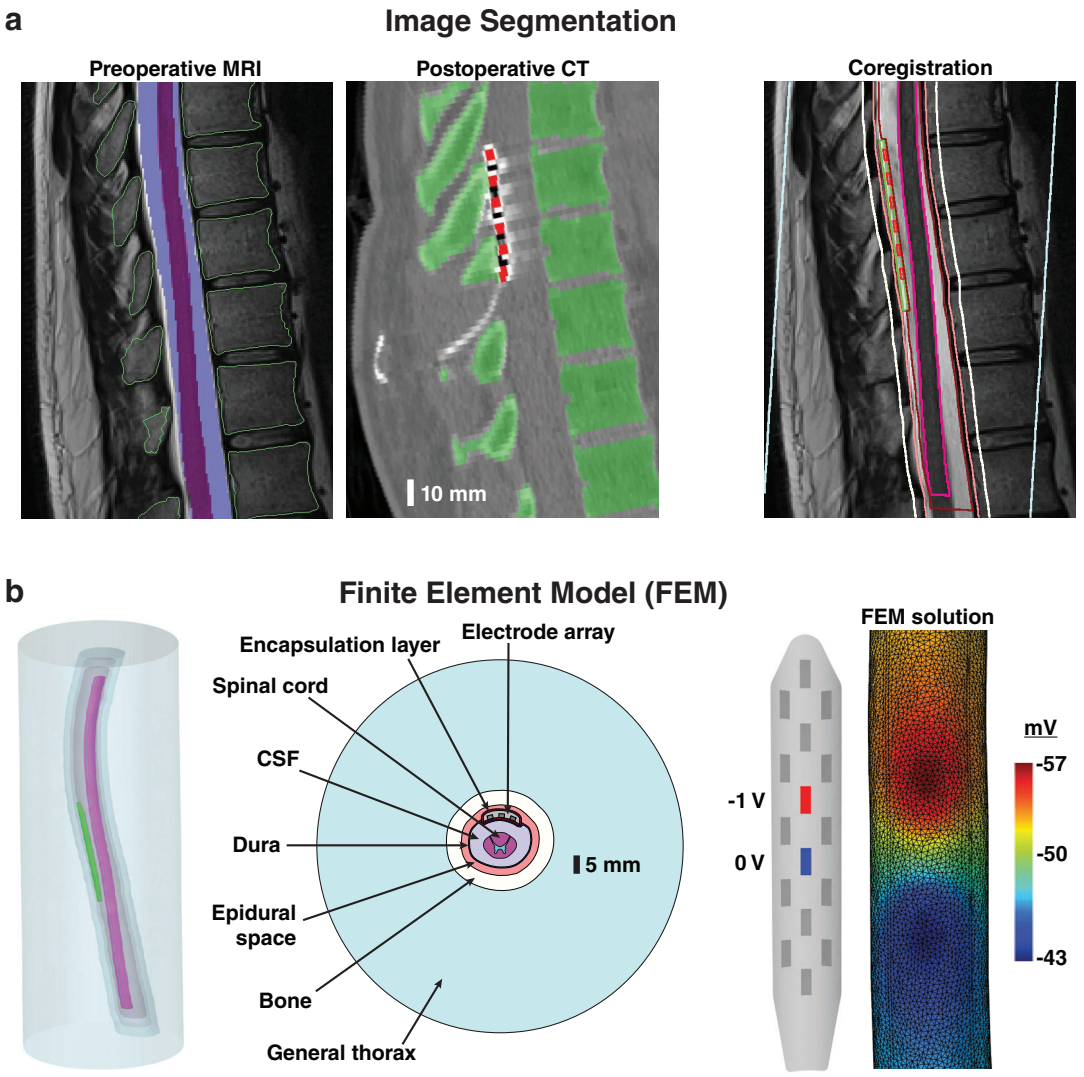

Figure 1. Patient-specific FEM. a. We used preoperative MRI scans to define the participant's anatomy (e.g., spinal cord, CSF, and spine) and a postoperative CT scan to define the 3D electrode locations. b. We coregistered the 3D objects segmented from the preoperative and postoperative images to define a patient-specific FEM. The figure on the top right shows outlines of the 3D FEM objects in the preoperative MRI. The figure on the bottom right shows the voltages generated on the surface of the spinal cord for a -1 V bipolar stimulus. (Note: In this figure, the electrode array and spinal cord are not drawn on the same scale.) [Color figure can be viewed at wileyonlinelibrary.com]

matched" model that, like the patient-specific FEM, included an additional domain to represent the electrode encapsulation.

We assigned electrical conductivities to each domain using experimental data available in the literature (12,14,34). For the patient-specific and the impedance-matched FEMs, we adjusted the encapsulation layer conductivity until each FEM produced average electrode impedances that matched the clinical impedance measurements. We applied 1 V and 0 V boundary conditions at the cathode and anode(s), respectively, set the outer tissue boundary of the FEM to be perfectly insulating and solved Laplace's equation. The corresponding spatially-dependent FEM voltage solutions were then scaled by the time-dependent output of the IPG to determine the spatiotemporal extracellular voltages generated by SCS (35,36).

Step 2: Define Axon Models in the Spinal Cord

The next step was to define computer models of spinal cord axons. With regards to SCS, studies have shown that the two axon types most likely affected by SCS are the large-diameter myelinated dorsal root (DR) fibers and Aβ fibers within the dorsal columns (DCs) (14,37). Therefore, we included computer models of both DR and DC fibers in our analysis (Fig. 2). We used a previously published compartmental model of a mammalian axon (38) to represent these axons. For both patient-specific and canonical models, we generated axon populations within the white matter boundaries of the spinal cord that covered a range of diameters (i.e., 5.7–11.5 μm) to match the axon diameters and densities measured in the DC of the human spinal cord (37,39). We also defined DR fibers that had a 3D axon trajectory in which they entered the spinal cord at a 45-degree angle (31). We placed DR fibers in 1-mm intervals along the rostrocaudal axis. Near the dorsal horn, the DR fiber branched into a daughter fiber that traveled within the DC along the rostrocaudal trajectory of the spinal cord.

Step 3: Assess the Axonal Response to SCS

The final step was to assess the axonal response to SCS under each set of conditions in our patient-specific and canonical models. We applied the extracellular voltages defined by the FEM

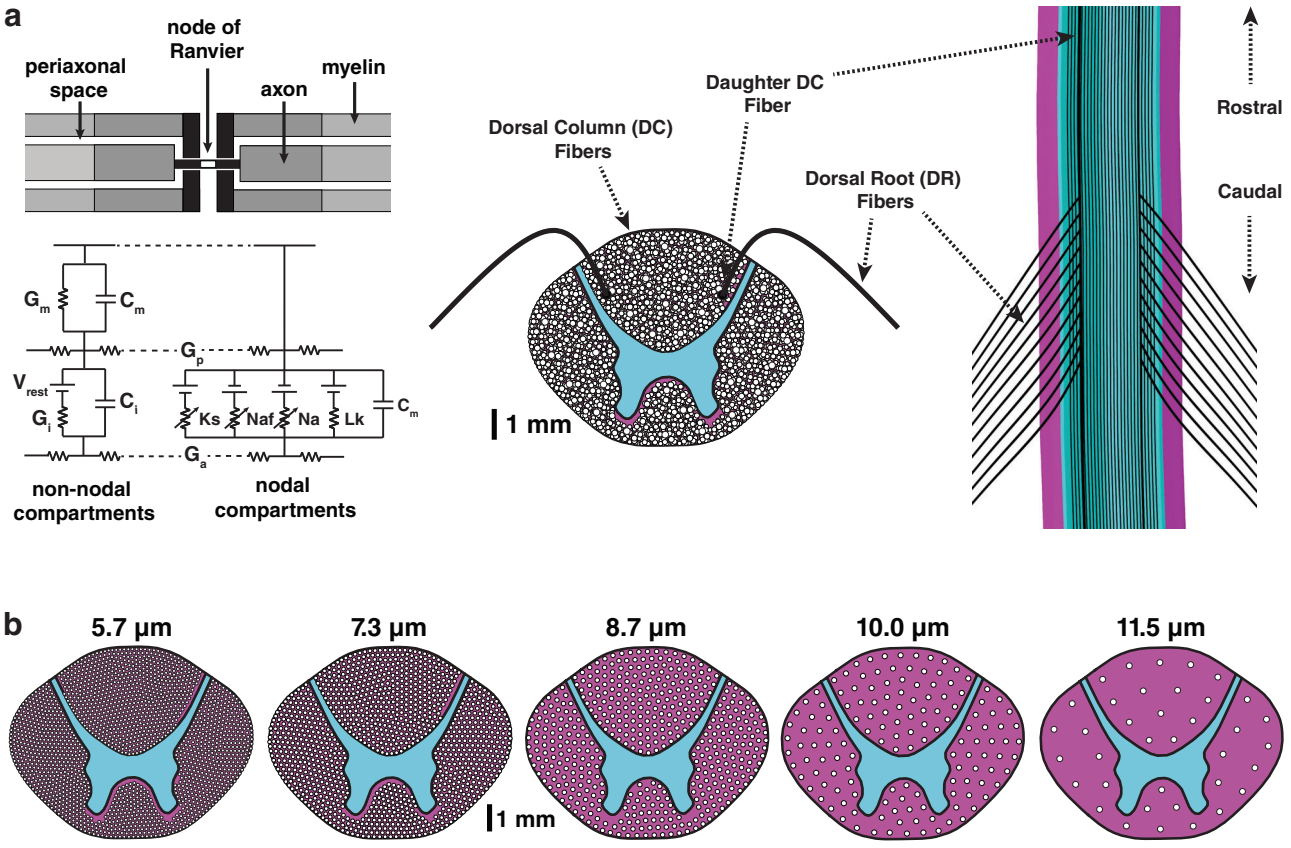

Figure 2. Axon models. a. In our analysis, we included multicompartment cable models of myelinated axons (38) running through the white matter of the spinal cord. We also included DR fibers that consisted of a mother fiber and a bifurcated daughter fiber running along the DCs. b. We generated axon populations that covered a range of diameters (i.e., 5.7–11.5 µm) to match the axon diameters and densities measured in the human spinal cord (37). For computational simplicity, we only used 1% of the true anatomical densities. (Note: In this figure, the axon diameters are not drawn to scale.) [Color figure can be viewed at wileyonlinelibrary.com]

(Step 1) to the axon models (Step 2) (Fig. 3). We then calculated the activation thresholds and a model-predicted ST for each parameter set and compared these model estimates to the corresponding clinical measurements.

Activation Threshold. We defined the activation threshold as the minimum pulse amplitude required to generate an action potential for each stimulus pulse in a particular axon.

Model ST. To compare our model predictions to our clinical measurements, we defined a model ST as the pulse amplitude required to activate ≥10% of the DC axons (11).

Pulse Width. We calculated the model ST for each pulse width that we tested clinically: 60, 210, 300, 450, and 1000 µs.

Stimulation Configuration. We calculated the activation thresholds and model ST for each stimulation configuration that we tested clinically: bipole, longitudinal guarded cathode, transverse guarded cathode, pseudo-monopole.

For a complete description of the model development and analysis, see the Supplemental Methods.

RESULTS

Fiber Size

Extracellular electrical stimulation can excite myelinated axons by generating action potentials at the nodes of Ranvier. For myelinated axons, the activation threshold is largely determined by the spacing between adjacent nodes of Ranvier (40). This internodal spacing increases as a function of axon diameter, and therefore large diameter fibers have a lower threshold than smaller fibers. Previous studies suggest that conventional SCS functions through direct activation of large-diameter myelinated axons within the DC (14). Therefore, fiber diameter is an important variable to consider because the DC in the human spinal cord consists of axons with a wide range of diameters (average axon diameter ~5.0 µm and a maximum diameter of 16.0 µm at lower thoracic levels) (37). Therefore, we calculated the activation thresholds for axon populations with a range of axon diameters (i.e., 5.7, 7.3, 8.7, 10.0, and 11.5 µm) and densities based on histological data from the human spinal cord (Fig. 4). For these simulations, we used a bipolar stimulation configuration, pulse width of 300 µs, and a pulse frequency of 50 Hz. The results displayed the expected trend of large-diameter fibers having the lowest activation thresholds.

In general, both canonical models exhibited significantly lower activation thresholds relative to the patient-specific model. According to these canonical models, a significant number of small diameter 5.7 µm axons were activated within the clinically-measured therapeutic range and even below the clinically-measured ST (Fig. 4). The patient-specific model predictions were more representative of the clinical findings and only predicted activation of these smaller diameter fibers at amplitudes above the clinically measured ST.

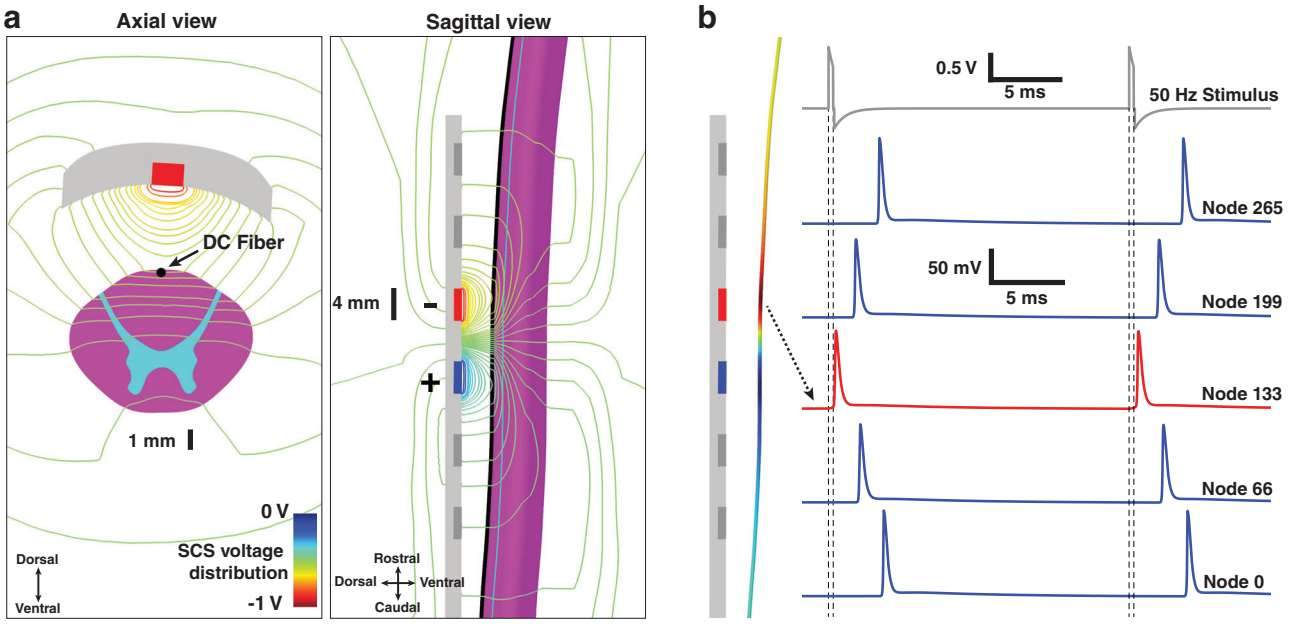

Figure 3. Axonal response to SCS. a. Axial and sagittal views of isopotential lines of the extracellular voltages generated by SCS. The voltage distributions were calculated from the patient-specific finite element model. b. To estimate the direct axonal response to SCS, we interpolated the SCS-induced extracellular voltages onto the axon models. With sufficient depolarization, action potentials were initiated in an axon and propagated in both orthodromic and antidromic directions. The figure shows the time-dependent transmembrane voltages at several nodes in a DC axon and illustrates action potential generation with a 50 Hz SCS waveform. [Color figure can be viewed at wileyonlinelibrary.com]

Pulse Width

For extracellular stimulation, increasing the pulse width leads to an exponential decrease in axonal activation thresholds (12). Clinical studies have demonstrated that increasing the pulse width can increase total paresthesia coverage, pain relief, and comfort (23,32). Therefore, we used the patient-specific and canonical models to estimate the ST as a function of pulse width. We defined the model-based ST as the minimum amplitude that produced activation of ≥10% of DC axons (11). We then compared the model-based ST to the clinically measured ST (Table 1). Both of the models and the clinical data exhibited an exponential decrease in ST with increasing pulse width (Fig. 5). The clinical ST was 6.6, 3.3, 2.7, 2.5, and 1.9 V for pulse widths of 60, 210, 300, 450, and 1000 μs, respectively. The patient-specific model ST was 7.5, 3.1, 2.6, 2.3, and 2.1 V with a mean absolute percentage error of 8.9% relative to the clinical ST. The canonical model ST was 3.9, 1.6, 1.4, 1.3, and 1.2 V with a mean absolute percentage error of 44.9% relative to the clinical ST. The impedance-matched canonical model ST was 5.8, 2.4, 2.0, 1.7, and 1.6 V with a mean absolute percentage error of 22.0% relative to the clinical ST.

We also calculated the minimum amplitudes required to activate DR fibers as a function of pulse width. In the patient-specific model, DR fiber activation started at 3.0, 1.4, 1.3, 1.2, and 1.1 V for pulse widths of 60, 210, 300, 450, and 1000 μs, respectively. In the canonical model, DR fiber activation started at 2.0, 1.0, 0.93, 0.85, and 0.85 V. In the impedance-matched canonical model, DR fiber activation started at 2.9, 1.4, 1.3, 1.1, and 1.1 V.

Stimulation Configuration

During SCS programming procedures, an extensive amount of time is dedicated to finding the combination of cathodes and anodes, also known as the stimulation configuration, that maximizes pain relief and minimizes side effects. Clinicians will select a variety of electrode combinations to "steer" the stimulation to generate an optimal paresthesia overlap. Therefore, we also considered the effects of changing the stimulation configuration on the clinical ST, CT, and DT and on model-predicted activation (Table 1). We tested the following stimulation configurations: bipole, longitudinal guarded tripole, transverse guarded tripole, and pseudo-monopole (Fig. 6). For the tested stimulation configurations, the clinical ST was 2.7, 2.2, 3.3, and 2.9 V, respectively. The patient-specific model ST was 2.6, 2.0, 2.4, and 3.1 V with a mean absolute percentage error of 12.1% relative to the clinical ST. The canonical model ST was 1.4, 1.0, 1.2, and 1.7 V with a mean absolute percentage error of 51.1% relative to the clinical ST. The impedance-matched canonical model ST was 2.0, 1.5, 1.8, and 2.4 V with a mean absolute percentage error of 30.8% relative to the clinical ST.

We also examined the extent of axonal activation predicted by the patient-specific model at the clinical CT and DT. The clinical CT was 4.1, 3.2, 5.0, and 4.3 V. The clinical DT was 5.9, 4.8, 6.4, and 5.8 V. At the clinical CT, the patient-specific model predicted extensive axonal activation within the DC, but activation of only 3.2, 3.1, 3.4, and 3.6% of axons within the dorsal lateral funiculi. At the clinical DT, the patient-specific model predicted considerable activation in the dorsal lateral funiculi of 10.6, 11.8, 7.2, and 11.1% of axons.

Furthermore, we calculated the minimum amplitudes required to activate DR fibers for each stimulation configuration. In the patient-specific model, DR fiber activation started at 1.3, 1.0, 1.3, and 1.2 V for each stimulation configuration. In the canonical model, DR fiber activation started at 0.93, 0.73, 0.93, and 0.95 V. In the impedance-matched canonical model, DR fiber activation started at 1.3, 1.0, 1.3, and 1.2 V.

DISCUSSION

The fundamental goal of this study was to develop a computer model that accounted for 3D patient-specific anatomy and

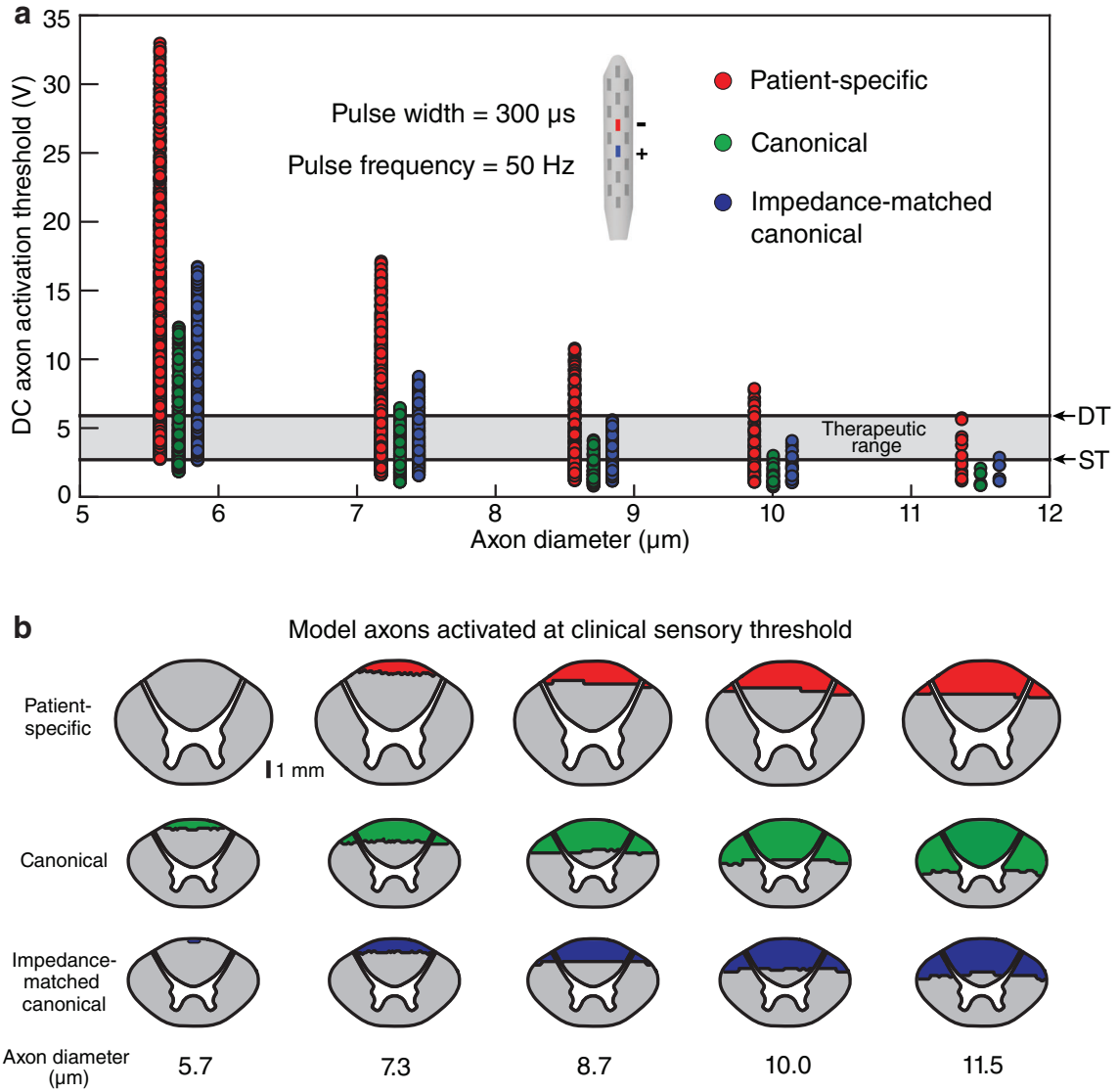

Figure 4. SCS activation thresholds as a function of axon diameter. a. Thresholds for individual axons within the DCs as a function of axon diameter. We performed simulations for the patient-specific and both canonical models. The clinical ST and DT are indicated by the black horizontal lines. b. Model axons activated at the clinical ST as a function of axon diameter. The top, middle, and bottom rows show axial cross sections of the spinal cord for the patient-specific, canonical, and impedance-matched canonical models, respectively. Activated axons are shown in red, green, and blue for the patient-specific, canonical, and impedance-matched canonical models, respectively. We calculated thresholds for a bipolar stimulation with a pulse width of 300 μs and a pulse frequency of 50 Hz. [Color figure can be viewed at wileyonlinelibrary.com]

Table 1. Clinical and Model-Based STs.

		Clinical ST	Patient-specific model ST	Canonical model ST	Impedance-matched canonical ST
Pulse width	60	6.6	7.5	3.9	5.8
	210	3.3	3.1	1.6	2.4
	300	2.7	2.6	1.4	2.0
	450	2.5	2.3	1.3	1.7
	1000	1.9	2.1	1.2	1.6
	MAPE		8.9%	44.9%	22.0%
Stimulation configuration	Bipole	2.7	2.6	1.4	2.0
	Longitudinal tripole	2.2	2.0	1.0	1.5
	Transverse tripole	3.3	2.4	1.2	1.8
	Pseudo-monopole	2.9	3.1	1.7	2.4
	MAPE		12.1%	51.1%	30.8%

ST, sensory threshold; MAPE, mean absolute percentage error.

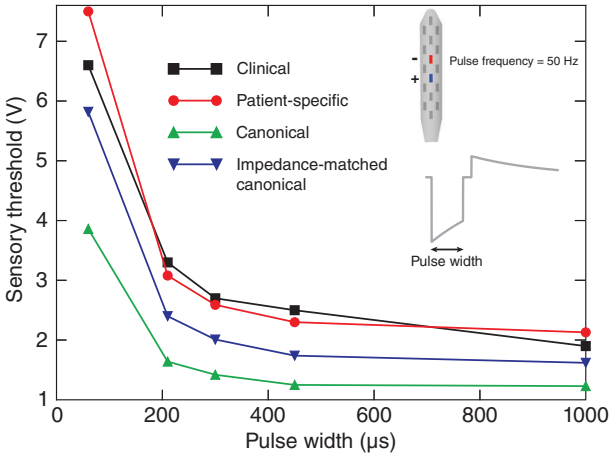

Figure 5. ST as a function of pulse width. We measured the clinical ST as a function of pulse width. We also estimated the model ST (i.e., minimum pulse amplitude to activate ≥10% of the DC axons) for the patient-specific and both canonical models. We calculated the ST for bipolar stimulation with a pulse frequency of 50 Hz. [Color figure can be viewed at wileyonlinelibrary.com]

electrode locations to investigate the direct neuromodulatory effects of SCS. To examine the significance of this patient-specific approach, we performed identical simulations with standard canonical models of SCS. Our results demonstrated considerable differences in axonal activation predicted with the patient-specific model relative to two canonical models. The canonical models predicted markedly lower thresholds for axonal activation (Figs. 4–6). The patient-specific model produced estimates of ST that were closer to the clinical ST measurements (Figs. 5 and 6). These results suggest that it is beneficial to consider sources of interpatient variability (e.g., anatomy and electrode locations) in computational analysis of SCS.

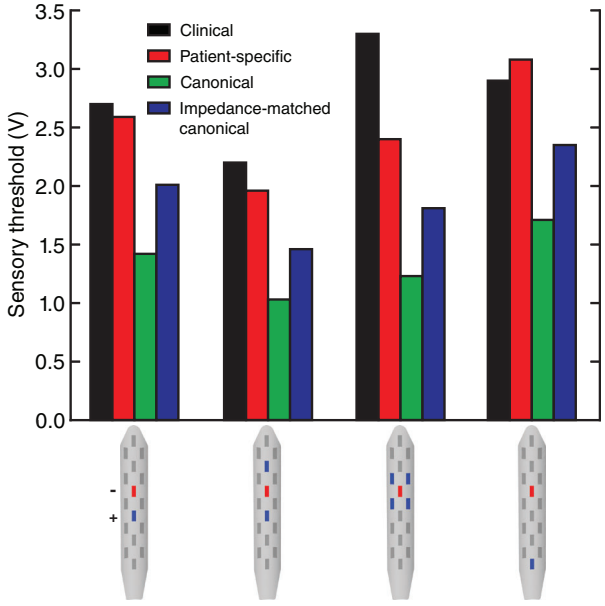

Figure 6. ST for various stimulation configurations. We measured the clinical ST and calculated the model ST (i.e., minimum pulse amplitude to activate ≥10% of the DC axons) for the patient-specific and both canonical models. We determined the ST for the following stimulation configurations: bipole (first column), longitudinal guarded cathode (second column), transverse guarded cathode (third column), and pseudo-monopole (fourth column). We determined the ST for a pulse width of 300 μs and a pulse frequency of 50 Hz. [Color figure can be viewed at wileyonlinelibrary.com]

We also considered the axonal activation predicted at clinical CT and DT. At CT, the patient-specific model predicted extensive activation of DC axons for several different stimulation configurations with little dorsolateral activation. However, at DT, the patient-specific model predicted that activation had spread to the dorsal lateral funiculi. Therefore, axons in the DR entry zone and Lissauer's tract, dorsal spinocerebellar tract, and lateral corticospinal tract may be activated at these stimulation amplitudes, contributing to patient discomfort.

The goal of this type of computational approach is to characterize the direct effects of SCS on different axonal pathways in the spinal cord. Canonical models based on averaged experimental and clinical measurements will continue to be an invaluable tool to improve our scientific understanding of SCS for pain and to improve lead design, stimulation configuration, and waveform parameters (9,10,12). However, the results of our study suggest that, under various conditions (e.g. patient anatomy, lead placement), patient-specific models may produce predictions of axonal activation within the spinal cord that are more consistent with clinical observations from individual patients. This study also suggests that patient-specific models capture the details necessary to quantitatively describe the axonal response to SCS. Therefore, these patient-specific models could help address scientific questions, such as therapeutic mechanisms of action, related to clinical SCS.

To better understand the mechanisms of action of SCS, it is critical that future research move toward patient-specific approaches to perform systematic studies of SCS in human subjects. One potential approach would be to couple patient-specific computational models with standard clinical outcome measures as well as objective measurements characterizing the physiological effects of SCS (e.g., quantitative sensory testing, functional neuroimaging) (4). This approach would help explain potential differences in the physiological effects of various SCS paradigms (e.g., tonic, burst, and kilohertz-frequency SCS). By accounting for additional sources of interpatient variability, patient-specific models would further highlight the potential advantages and disadvantages of various lead designs, lead placements, and stimulation configurations. These patient-specific models could also be used to investigate changes in neural activity associated with spinal cord movement (e.g., due to body position, respiration, and cough) that are being considered in a novel closed-loop SCS system (39,41,42). We believe that this type of patient-specific approach will further elucidate the physiological and technical factors relevant to SCS to improve implementation of current systems as well as innovate novel technologies to significantly improve the clinical outcomes associated with SCS.

Although the results of this study exhibited excellent agreement between the patient-specific model and clinical measurements, this study had several limitations. This study was a proof-of-concept study performed in a single patient. The true validity and utility of this type of approach needs to be validated by extending this approach to multiple patients and testing a wider range of waveform parameters and stimulation configurations. To help make this patient-specific approach feasible, a cohort study would account for multiple sources of interpatient variability and allow for a parameter sensitivity analysis to determine the minimal model complexity necessary to produce accurate model-based predictions. We also assumed that model-based ST corresponded to activation of ≥10% of the DC axons. While this approach has been used in previous SCS modeling studies (11,15), other modeling studies have suggested that ST

corresponds to the activation of only a single large-diameter DC fiber (14). Therefore, in future studies, it will be critical to examine what degree of model-based activation best correlates with clinical measurements in a large cohort. Furthermore, we only performed clinical measurements for acute SCS and did not correlate model predictions of axonal activation with clinical outcomes (i.e. pain relief over time). We also tested several sets of stimulation parameters within a single research visit; therefore, it is possible that carryover effects could have influenced the thresholds for individual sets of stimulation parameters. Due to the limited resolution of the clinical MRI scan, we were unable to define patient-specific gray- and white-matter boundaries in the spinal cord and we had to define these boundaries from a cadaver sample (43) that was scaled to match the outer dimensions of the patient's spinal cord. However, it is possible that future improvements in diffusion tensor imaging and fiber tractography could help address this limitation. Another potential limitation was that our axon distributions were based on a study that only considered the superficial (~300 μm) aspect of the DC (37). Other white matter areas may have different fiber size distributions and therefore different activation thresholds. However, previous studies have shown that the large-diameter myelinated axons in the superficial DC have the lowest thresholds to SCS (13,14,16). In our models, we represented the electrical properties of the tissue as purely resistive. The capacitive properties of biological tissues could affect the spatiotemporal voltages generated during SCS and the corresponding neural response, especially at higher stimulation frequencies. However, previous studies suggest that tissue capacitance has a negligible filtering effect with conventional SCS parameters, especially during voltage-controlled stimulation (44–46).

One of the main limitations was estimating DR fiber activation. DR fiber activation can generate uncomfortable paresthesias and/or activation of motor reflex nerves before sufficient activation of DC fibers. One goal of SCS modeling is to guide the selection of stimulation configurations and waveform parameters that selectively activate DC fibers over DR fibers. In our models, DR fiber activation occurred at amplitudes below the clinical ST. DR thresholds were lowest for fibers that entered the spinal cord near the cathode and the thresholds rapidly increased for fibers a few millimeters above or below the cathode (data not shown). For the bipole configuration, there was also a decrease in activation threshold for DR fibers entering the spinal cord near the anode. We believe that the low thresholds for DR fiber activation were partly attributed to the FEM design. To reduce computational demands, the anatomy of the rootlets is typically not represented in the FEM mesh (Figs. 1 and 3) (14). However, the rootlets have a lower electrical conductivity relative to the surrounding CSF. Therefore, our model, along with the models used in several other studies, may overestimate the excitability of DR fibers for a given fiber size. Future studies should consider explicitly representing the spinal cord rootlets within the FEM (47). With regards to neural activation at DT, future studies should also consider the range of diameters, number of fibers, as well as functional groups (e.g. proprioceptive, touch) of DR fibers that are activated at stimulation settings that produce unwanted side effects.

To improve the accuracy of the model-based estimations of the voltage distributions generated in the spinal cord, we developed a circuit model of the output of the clinical neurostimulator utilized in this study that we coupled to each FEM (see Supplemental Methods) (36). We used this approach to account for differences in the tissue voltages generated by standard clinical neurostimulators as a function of pulse width and pulse frequency. In the patient-specific and impedance-matched canonical models, we adjusted the electrical conductivity of the encapsulation layer domain so that the model impedances matched the average impedances measured by the clinical programming device. In this study, matching the model impedance to the clinical impedance was important because the relevant commercial SCS system utilized voltage-controlled stimulation. Electrode impedance variability can produce large differences in the tissue voltages generated during voltage-controlled stimulation (48). In this study, we only considered a single encapsulation layer domain that would not be able to account for potential electrical heterogeneities in the tissue surrounding individual electrodes. In a previous SCS modeling study, these potential heterogeneities were shown to affect the 3D voltage distributions and corresponding activation within the spinal cord (29). While our current methodology only permitted us to account for the average electrode impedance, it would be possible to include local encapsulation layer domains at and around each individual electrode (29). This approach would provide a means to consider electrical heterogeneities and to adjust the model parameters so that each model impedance matched the corresponding clinical impedance for each individual electrode. It should also be noted that while the commercial SCS system considered in this study utilized voltage-controlled stimulation, many SCS systems utilize current-controlled stimulation that would reduce the potential effects of the electrode encapsulation and heterogeneities on the corresponding voltage distributions generated within the spinal cord (48–50).

CONCLUSIONS

In this study, we implemented a patient-specific computer modeling approach of SCS. By accounting for patient-specific anatomy, electrode locations, and impedances, theoretical estimates of SCS-induced neuromodulation closely matched the corresponding clinical measurements with far greater accuracy than predictions from standard canonical models. These results suggest that patient-specific models can provide quantitative descriptions of the neural response to SCS and serve as a tool to address scientific questions related to clinical SCS as well as inform the development of tools that may guide SCS implantation and programming.

Acknowledgments

Scott F. Lempka would like to thank Fang Dong (Cleveland Clinic, Cleveland, OH, USA) for help developing the X-ray CT protocol, Stephen E. Jones (Cleveland Clinic) for assistance with image segmentation, and Kabilar Gunalan (Case Western Reserve University, Cleveland, OH, USA) for assistance with computer simulations. Scott F. Lempka would also like to thank Cameron C. McIntyre (Case Western Reserve University) and Vishwanath Sankarasubramanian and Robert Graham (University of Michigan) for helpful comments and discussion.

Authorship Statements

All authors were responsible for the study concept and design. Scott F. Lempka and John G. Ozinga performed the data acquisition. Scott F. Lempka, Hans J. Zander, and Carlos J. Anaya performed the model design. Scott F. Lempka performed the model analysis. Scott F. Lempka prepared the manuscript draft, figures, and table with guidance from Alexandria Wyant, John G. Ozinga, and Andre G. Machado. All authors provided intellectual input and assisted with manuscript revisions. All authors approved the final version of the manuscript.

How to Cite this Article:

Lempka S.F., Zander H.J., Anaya C.J., Wyant A., Ozinga J.G., Machado A.G. 2020. Patient-Specific Analysis of Neural Activation During Spinal Cord Stimulation for Pain. Neuromodulation 2020; 23: 572–581

REFERENCES

1. North RB, Kidd DH, Piantadosi S. Spinal cord stimulation versus reoperation for failed back surgery syndrome: a prospective, randomized study design. *Acta Neurochir* 1995;64:106–108.
2. Kemler MA, Barendse GA, van Kleef M et al. Spinal cord stimulatoin in patients with chronic reflex sympathetic dystrophy. *N Engl J Med* 2000;343:618–624.
3. Kumar K, Taylor RS, Jacques L et al. The effects of spinal cord stimulation in neuropathic pain are sustained: a 24-month follow-up of the prospective randomized controlled multicenter trial of the effectiveness of spinal cord stimulation. *Neurosurgery* 2008;63:762–770. https://doi.org/10.1227/01.NEU.0000325731.46702.D9.
4. Sankarasubramanian V, Harte SE, Chiravuri S et al. Objective measures to characterize the physiological effects of spinal cord stimulation in neuropathic pain: a literature review. *Neuromodulation* 2018;22(2):127–148. https://doi.org/10.1111/ner.12804.
5. Guan Y, Wacnik PW, Yang F et al. Spinal cord stimulation-induced analgesia. *Anesthesiology* 2010;113:1392–1405. https://doi.org/10.1097/ALN.0b013e3181fcd95c.
6. Song Z, Meyerson BA, Linderoth B. Spinal 5-HT receptors that contribute to the pain-relieving effects of spinal cord stimulation in a rat model of neuropathy. *Pain* 2011;152:1666–1673. https://doi.org/10.1016/j.pain.2011.03.012.
7. Zhang TC, Janik JJ, Peters RV, Chen G, Ji R-R, Grill WM. Spinal sensory projection neuron responses to spinal cord stimulation are mediated by circuits beyond gate control. *J Neurophysiol* 2015;114:284–300. https://doi.org/10.1152/jn.00147.2015.
8. Youn Y, Smith H, Morris B, Argoff C, Pilitsis JG. The effect of high-frequency stimulation on sensory thresholds in chronic pain patients. *Stereotact Funct Neurosurg* 2015;93:355–359. https://doi.org/10.1159/000438998.
9. Holsheimer J, Wesselink WA. Effect of anode-cathode configuration on paresthesia coverage in spinal cord stimulation. *Neurosurgery* 1997;41:654–660.
10. Struijk JJ, Holsheimer J. Transverse tripolar spinal cord stimulation: theoretical performance of a dual channel system. *Med Biol Eng Comput* 1996;34:273–279.
11. Howell B, Lad SP, Grill WM. Evaluation of intradural stimulation efficiency and selectivity in a computational model of spinal cord stimulation. *PLoS One.* 2014;9:e114938. https://doi.org/10.1371/journal.pone.0114938.
12. Lee D, Hershey B, Bradley K, Yearwood T. Predicted effects of pulse width programming in spinal cord stimulation: a mathematical modeling study. *Med Biol Eng Comput* 2011;49:765–774. https://doi.org/10.1007/s11517-011-0780-9.
13. Lee D, Gillespie E, Bradley K. Dorsal column steerability with dual parallel leads using dedicated power sources: a computational model. *J Vis Exp* 2011. https://doi.org/10.3791/2443.
14. Holsheimer J. Which neuronal elements are activated directly by spinal cord stimulation. *Neuromodulation.* 2002;5:25–31. https://doi.org/10.1046/j.1525-1403.2002._2005.x.
15. Capogrosso M, Wenger N, Raspopovic S et al. A computational model for epidural electrical stimulation of spinal sensorimotor circuits. *J Neurosci* 2013;33:19326–19340. https://doi.org/10.1523/JNEUROSCI.1688-13.2013.
16. Lempka SF, McIntyre CC, Kilgore KL, Machado AG. Computational analysis of kilohertz frequency spinal cord stimulation for chronic pain management. *Anesthesiology* 2015;122:1362–1376. https://doi.org/10.1097/ALN.0000000000000649.
17. Zhang TC, Janik JJ, Grill WM. Modeling effects of spinal cord stimulation on wide-dynamic range dorsal horn neurons: influence of stimulation frequency and GABAergic inhibition. *J Neurophysiol* 2014;112:552–567. https://doi.org/10.1152/jn.00254.2014.
18. Holsheimer J, den Boer JA, Struijk JJ, Rozeboom AR. MR assessment of the normal position of the spinal cord in the spinal canal. *AJNR Am J Neuroradiol* 1994;15:951–959.
19. Delmotte A, Jacques L, Kumar K et al. The Franco-Canadian multicolumn spinal cord stimulation prospective study: a subgroup analysis focusing on the decisive role of lead positioning. *Neurochirurgie* 2015;61:S83–S89. https://doi.org/10.1016/j.neuchi.2014.06.005.
20. Struijk JJ, Holsheimer J, Barolat G, He J, Boom HBK. Paresthesia thresholds in spinal cord stimulation: a comparison of theoretical results with clinical data. 1993;I:101–108.
21. Barolat G, Ketcik B, He J. Long-term outcome of spinal cord stimulation for chronic pain management. *Neuromodulation* 1998;1:19–29.
22. Aló KM, Redko V, Charnov J. Four year follow-up of dual electrode spinal cord stimulation for chronic pain. *Neuromodulation* 2002;5:79–88.
23. Yearwood TL, Hershey B, Bradley K, Lee D. Pulse width programming in spinal cord stimulation: a clinical study. *Pain Physician* 2010;13:321–335.
24. He J, Barolat G, Holsheimer J, Struijk JJ. Perception threshold and electrode position for spinal cord stimulation. *Pain* 1994;59:55–63. https://doi.org/10.1016/0304-3959(94)90047-7.
25. Chaturvedi A, Butson CR, Lempka SF, Cooper SE, McIntyre CC. Patient-specific models of deep brain stimulation: influence of field model complexity on neural activation predictions. *Brain Stimul* 2010;3:65–77. https://doi.org/10.1016/j.brs.2010.01.003.
26. Frankemolle AMM, Wu J, Noecker AM et al. Reversing cognitive-motor impairments in Parkinson's disease patients using a computational modelling approach to deep brain stimulation programming. *Brain* 2010;133:746–761. https://doi.org/10.1093/brain/awp315.
27. Lujan JL, Chaturvedi A, Malone DA, Rezai AR, Machado AG, Mcintyre CC. Axonal pathways linked to therapeutic and nontherapeutic outcomes during psychiatric deep brain stimulation. *Hum Brain Mapp* 2012;33:958–968. https://doi.org/10.1002/hbm.21262.
28. McIntyre CC, Chaturvedi A, Shamir RR, Lempka SF. Engineering the next generation of clinical deep brain stimulation technology. *Brain Stimul* 2015;8:21–26. https://doi.org/10.1016/j.brs.2014.07.039.
29. Arle JE, Carlson KW, Mei L, Shils JL. Modeling effects of scar on patterns of dorsal column stimulation. *Neuromodulation.* 2014;17:320–333. https://doi.org/10.1111/ner.12128.
30. Kumar K, Taylor RS, Jacques L et al. Spinal cord stimulation versus conventional medical management for neuropathic pain: a multicentre randomised controlled trial in patients with failed back surgery syndrome. *Pain* 2007;132:179–188. https://doi.org/10.1016/j.pain.2007.07.028.
31. Struijk JJ, Holsheimer J, Boom HBK. Excitation of dorsal root fibers in spinal cord stimulation: a theoretical study. *IEEE Trans Biomed Eng* 1993;40:632–639.
32. Holsheimer J, Buitenweg JR, Das J, De Sutter P, Manola L, Nuttin B. The effect of pulse width and contact configuration on paresthesia coverage in spinal cord stimulation. *Neurosurgery* 2011;68:1452–1461. https://doi.org/10.1227/NEU.0b013e31820b4f47.
33. Sankarasubramanian V, Buitenweg JR, Holsheimer J, Veltink PH. Staggered transverse tripoles with quadripolar lateral anodes using percutaneous and surgical leads in spinal cord stimulation. *Neurosurgery* 2013;72:483–491. https://doi.org/10.1227/NEU.0b013e31827d0e12.
34. Ladenbauer J, Minassian K, Hofstoetter US, Dimitrijevic MR, Ratty F. Stimulation of the human lumbar spinal cord with implanted and surface electrodes—a computer simulation study. *IEEE Trans Neural Syst Rehabil Eng* 2010;18:637–645.
35. Gunalan K, Chaturvedi A, Howell B et al. Creating and parameterizing patient-specific deep brain stimulation pathway-activation models using the hyperdirect pathway as an example. *PLoS One* 2017;12:e0176132.
36. Lempka SF, Howell B, Gunalan K, Machado AG, McIntyre CC. Characterization of the stimulus waveforms generated by implantable pulse generators for deep brain stimulation. *Clin Neurophysiol* 2018;129:731–742. https://doi.org/10.1016/j.clinph.2018.01.015.
37. Feirabend HKP, Choufoer H, Ploeger S, Holsheimer J, van Gool JD. Morphometry of human superficial dorsal and dorsolateral column fibres: significance to spinal cord stimulation. *Brain* 2002;125:1137–1149.
38. McIntyre CC, Richardson AG, Grill WM. Modeling the excitability of mammalian nerve fibers: influence of afterpotentials on the recovery cycle. *J Neurophysiol* 2002;87:995–1006.
39. Anaya, C. J., Zander, H. J., Graham, R. D., Sankarasubramanian, V., & Lempka, S. F. (2019). Evoked Potentials Recorded From the Spinal Cord During Neurostimulation for Pain: A Computational Modeling Study. *Neuromodulation: Technology at the Neural Interface*. https://doi.org/10.1111/ner.12965
40. Rattay, F. (1986). Analysis of Models for External Stimulation of Axons. *IEEE Transactions on Biomedical Engineering*, BME-33(10), 974–977. https://doi.org/10.1109/tbme.1986.325670
41. Parker JL, Karantonis DM, Single PS, Obradovic M, Cousins MJ. Compound action potentials recorded in the human spinal cord during neurostimulation for pain relief. *Pain* 2012;153:593–601. https://doi.org/10.1016/j.pain.2011.11.023.
42. Russo M, Cousins MJ, Brooker C et al. Effective relief of pain and associated symptoms with closed-loop spinal cord stimulation system: preliminary results of the Avalon study. *Neuromodulation* 2018;21:38–47. https://doi.org/10.1111/ner.12684.
43. Kameyama T, Hashizume Y, Sobue G. Morphologic features of the normal human cadaveric spinal cord. *Spine (Phila Pa 1976)* 1996;21:1285–1290.
44. Plonsey R, Heppner DB. Considerations of quasi-stationarity in electrophysiological systems. *Bull Math Biophys* 1967;29:657–664. https://doi.org/10.1007/BF02476917.
45. Butson CR, McIntyre CC. Tissue and electrode capacitance reduce neural activation volumes during deep brain stimulation. *Clin Neurophysiol* 2005;116:2490–2500. https://doi.org/10.1016/j.clinph.2005.06.023.
46. Bossetti CA, Birdno MJ, Grill WM. Analysis of the quasi-static approximation for calculating potentials generated by neural stimulation. *J Neural Eng* 2008;5:44–53. https://doi.org/10.1088/1741-2560/5/1/005.
47. Wagner FB, Mignardot J, Le G-m CG et al. Targeted neurotechnology restores walking in humans with spinal cord injury. *Nature* 2018;563:65–71. https://doi.org/10.1038/s41586-018-0649-2.
48. Lempka SF, Johnson MD, Miocinovic S, Vitek JL, Mcintyre CC. Current-controlled deep brain stimulation reduces in vivo voltage fluctuations observed during

voltage-controlled stimulation. *Clin Neurophysiol* 2010;121:2128–2133. https://doi.org/10.1016/j.clinph.2010.04.026.
49. Miocinovic S, Lempka SF, Russo GS et al. Experimental and theoretical characterization of the voltage distribution generated by deep brain stimulation. *Exp Neurol* 2009;216:166–176. https://doi.org/10.1016/j.expneurol.2008.11.024.
50. Lempka SF, Patil PG. Innovations in spinal cord stimulation for pain. *Curr Opin Biomed Eng* 2018;8:51–60. https://doi.org/10.1016/j.cobme.2018.10.005.

SUPPORTING INFORMATION

Additional supporting information may be found online in the supporting information tab for this article.

COMMENT

This work shows what is now becoming evident, that patient-specific anatomy can substantially influence the therapeutic outcomes of Neuromodulation therapies. Only computer models like the one proposed here can help understanding if the current approach of a one-fit-all technology is still valuable.

Marco Capogrosso, PhD
Pittsburgh, PA USA

Comments not included in the Early View version of this paper.

